

Characterizing Standing Postural Coordination Across the Reaching Workspace With A Six-Degree-of-Freedom Biomechanical Model

Robert M. Carrera¹, Yupei Cai¹, Keshu Cai¹, Xiangzhi Zhao¹, Aaryaman Chandgothia¹, Isirame Omofuma¹, Utkarsh Kotekal¹, Arihant Yadav¹, Apurva Reddy¹, Sunil K. Agrawal^{1,†}

Abstract—Standing reach tasks are commonly used in postural rehabilitation, yet normative postural coordination patterns in unimpaired subjects have not been well characterized. Understanding these patterns could help clinicians identify postural coordination deficits or place reaching targets to train specific muscle groups or postural strategies. 16 unimpaired subjects completed a unilateral maximal reaching task in virtual reality (VR). Subjects used their right arm to push targets at 4 heights as far as possible along 5 directions ranging from rightwards to forwards. We used a 6-degree-of-freedom kinematic model to describe pelvis and chest translations, separately analyzed pelvis and chest orientation, and evaluated the contribution of the model and orientation variables to the movement of the reaching arm's shoulder. Similar chest and shoulder trajectories were observed between subjects. For all reach targets, forward and downward shoulder movement were driven by pelvis-chest angles. Ankle-pelvis angles contributed significantly to lateral shoulder movement, especially for higher lateral targets. Moving the shoulder downward to lower targets required the use of smaller ankle-pelvis angles to "counterbalance" greater pelvis-chest angles and larger torso center of mass (COM) excursion. Pelvic tilt and, to a lesser extent, lumbothoracic flexion played a critical role in moving the shoulder forward and downward, especially for lower targets. Rightward pelvic rotation and pelvic tilt acted together to direct the shoulder toward low rightward targets. The results show how postural coordination supports upper limb tasks, highlight how movement limitations could impact the reaching workspace, and provide insights for the development of postural rehabilitation tasks.

I. INTRODUCTION

For those with postural control deficits, standing postural control training can help improve functional independence and mobility. For people with upper motor neuron dysfunction, it can help improve muscle strength, reduce spasticity, stretch contracted muscles, improve bladder function, and hasten a return to walking [1], [2].

In-place postural control training can range from weight-bearing and maintaining postural alignment to more dynamic tasks such as leaning and reaching for targets or performing other goal-oriented upper limb tasks [3], [4]. Knowledge of the normative postural coordination of standing reach could help therapists target muscle groups at involved joints, place targets to appropriately challenge a subject's range of motion and

This work was partially supported by the Spinal Cord Injury Board of the New York State Department of Health under award number C3XXX.

¹Mechanical Engineering, Columbia University, New York, NY USA.

† Corresponding author: sa3077@columbia.edu

strength limitations, identify restrictions in multi-segment and multi-joint coordination patterns, or re-train normative coordination patterns. An understanding of the typical contribution of specific degrees of freedom to the reaching workspace could also be useful in understanding how movement limitations, such as reduced lumbothoracic axial rotation and lateral bending in the elderly or reduced trunk control in cerebral palsy, could impact the reaching workspace [5], [6]. Despite the potential clinical utility, few studies have reported descriptions of observed postural kinematics in reaching.

In seated reaching, torso axial rotation plays an important role for targets at about 50° or more from the forward direction [7], [8]. When seated in a car, older subjects preferred keeping the elbow closer to the trunk during lateral and overhead reaches as compared to younger subjects, perhaps reducing shoulder joint loading [9]. In seated reach, the involvement of the pelvis and torso in a reach can be roughly predicted based on four target reaching zones [10].

Studies of standing reaching have been limited to reaching targets at a single height or in the sagittal plane. Older subjects were found to have reduced torso axial rotation and trunk flexion when performing a self-paced maximal reach to a target at the level of the acromion process in the sagittal plane [11]. Most subjects use a "hip strategy" involving little ankle plantarflexion and substantial hip flexion when reaching forward in the Functional Reach Test (FRT) [5]. Multiobjective optimization (MOO) methods used to predict posture often focus on prediction accuracy, without reporting details of the observed or predicted reaching postures [12], [13].

In this work, we used a 6-DoF kinematic model to characterize typical postural coordination when reaching for targets in different directions and at different heights in virtual reality (VR). The model extends the double-inverted pendulum model of stance to provide a complete description of the relative positions of the mid-ankle, pelvis, and chest [14], [15]. We first analyzed the similarity of the pelvis, chest, and shoulder during a reach to a given target, as a postural coordination pattern can only be described as "normative" if subjects exhibit similar postural coordination patterns.

Gaze, stance, and the purpose of the reach can have important effects on postural coordination. During reaching, both the gaze and the reach must be directed to the target and people select a postural coordination that achieves both objectives [16]. Whether the reach involves a load, whether the load has to be held statically or transported, and the load mass can also substantially affect selected posture [17]. Subjects performed the task presented here at a shoulder-width stance, with no

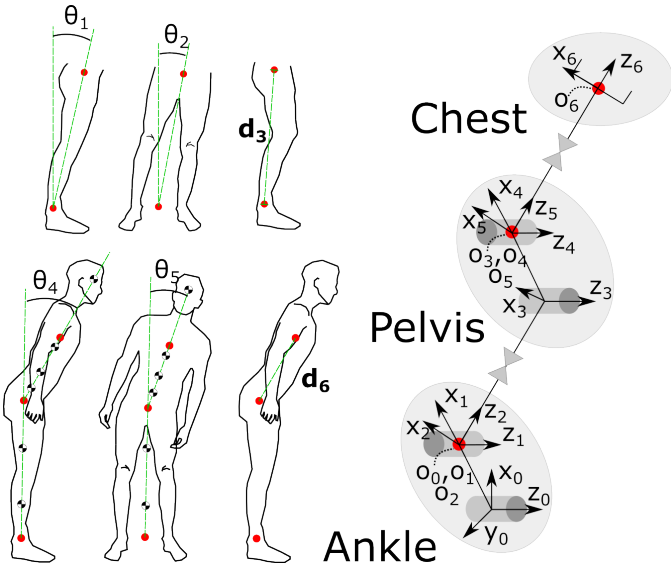


Fig. 1. The 6-DoF model for characterizing ankle-pelvis-chest relative positioning. The first model link represents the lower limbs and the second represents the torso and upper body. Links are shown as green dotted lines connecting red circles on the subject silhouettes and as black lines linking shaded regions in the kinematic model diagram. Link masses and center of mass (COM) positions (circles with two shaded quadrants on the θ_4 and θ_5 silhouettes) were computed from the marker data and published anthropometric data. The lower limb link mass incorporated the shank and thigh masses. The upper body link mass incorporated a 3-segment torso, the upper extremity masses which were evenly distributed over the 3 torso COMs, and the head mass.

load, and without visual obstructions, a common scenario in daily life and in standing rehabilitation tasks.

Beyond reporting observed joint variables, we also characterized the contribution of each model joint variable and orientation variable to the movement of the shoulder of the reaching arm. This approach quantifies the importance of specific degrees of freedom to the reaching workspace. By assigning model dynamic properties such as mass and segment COM position using reported anthropometrics, we also show how small ankle-pelvis angle changes with target height play a critical role in enabling larger pelvis-chest angles needed to reach low targets.

II. METHODS

A. Experimental Procedure

16 subjects without neurological or musculoskeletal impairment and ranging in age from 21 to 29 years performed a virtual reality (VR) task in which they were asked to push floating targets as far outwards as possible (see supplemental video). Participants gave informed consent under Columbia University IRB protocol AAAR6780. The Vicon motion tracking system captured the movement of 49 retroreflective markers on the lower limbs, pelvis, chest, shoulder, and upper limbs. Subjects stood with the outer edges of the feet at shoulder width. Green, spherical reaching targets were placed at a distance of 70% of the summed upper arm and forearm length from the subject along five directions: rightwards or 0° , 22.5° , front-right or 45° , 67.5° , and forwards or 90° . Subjects used a marker placed on the ulnar head to "slide" targets outwards along a target

travel vector. This vector was contained within a transverse plane at the vertical height of the target and oriented from the center of the base of support (BoS) to the target's initial position. The center of the BoS had an anteroposterior (AP) component at the mean position of bilateral markers on the heels and distal phalanges of the 1st digit. The BoS center mediolateral (ML) component was the midpoint of bilateral markers on the 5th metatarsal head. The ulnar marker was rendered in the VR environment using a transformation matrix relating the Vicon and VR coordinate systems.

Reaching targets were placed at heights corresponding to the pelvis, chest, shoulder, and eye. The heights for ball placement were determined from the initial position of markers when the subject stood in a neutral pose. The pelvic height was that of the center of 4 markers placed on the left and right posterior and anterior superior iliac spines. The chest height was that of the center of 2 ventral markers and 2 dorsal markers placed at the level of the inferior angle of the scapula. The shoulder height was the midpoint of two markers placed bilaterally on the acromion processes. The eye-level height was the shoulder height plus the vertical distance from the shoulder to the eye, which was measured manually. Subjects completed 3 trials for each reach direction/height combination.

B. Kinematic Model Definition

The kinematic model is depicted in Fig. 2. The model has 3 DoF between the mid-ankle and mid-pelvis positions: two rotational DOF at the ankle joint center and a length representing the distance from the mid-ankle point to the pelvic center (d_3). These model joint variables relate the positions of the mid-ankle and pelvis. Similarly, the model has 3 DoF between the mid-pelvis and mid-chest positions: two rotational DOF at the mid-pelvis and a length representing the distance from the pelvis to the chest position (d_6). The Denavit-Hartenberg (DH) parameters describing the model, provided in the supplemental material, can be used to easily recreate the model with robot modeling software such as MATLAB's robotics toolkit. The descriptions of the relative ankle-pelvis and pelvis-chest displacements are similar to

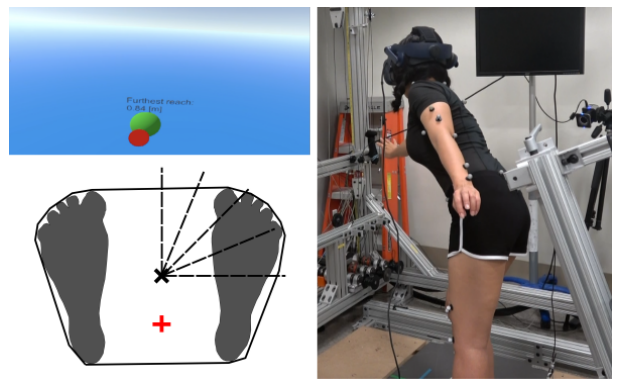


Fig. 2. Clockwise from top left: a view of the task as seen by a subject; a subject performing a waist-level, front-rightward reach; a schematic showing the feet enclosed by the base of support (BoS; black line), center of the BoS (black cross) and ankles (red cross), and the five target travel directions which radiate from the BoS center (dashed black lines).

spherical coordinates, with the important caveat that, due to the serial nature of the model, joint variables more proximal to the ankle affect the axes of rotation of more distal joints. However, ankle-pelvis angles were generally quite small. As a result, θ_1 and θ_2 closely reflect AP and ML movement of the pelvis relative to the ankle and θ_4 closely reflects AP movement of the chest relative to the pelvis. On the other hand, θ_5 likely contributed substantially to both AP and ML chest movement, as θ_4 values were often large. As a result, we consider the combined contribution of θ_4 and θ_5 to the reaching shoulder's movement in the discussion.

The model joint variables describing two relative positions incorporate the movements of the intervening anatomic joints. The model joint variables describing the pelvis position relative to the mid-ankle, namely θ_1 , θ_2 , and d_3 , reflect ankle plantar/dorsiflexion, ankle inversion/eversion, knee flexion/extension, and pelvic orientation. The model joint variables describing the chest position relative to the pelvis, θ_4 , θ_5 , and d_6 , reflect pelvic orientation and flexion/extension, axial rotation, and lateral bending of the lumbothoracic spine.

C. Motion Tracking, Inverse Kinematics, and Orientation Descriptions

We used the dynamic precision method to select a subject-specific cutoff frequency for a 4th-order low-pass Butterworth filter applied to the marker data [18]. In brief, the dynamic precision method selects the cutoff frequency that minimizes the mean of the computed standard deviations (STD) of the distance between all pairs of raw and filtered markers on a rigid body. For n markers placed on a rigid body, the cutoff frequency is chosen that minimizes σ_{dist} , where

$$\sigma_{dist} = \sum_{i=1}^{n-1} \sum_{j=i+1}^n (\sigma_{i_r,j_f} + \sigma_{i_f,j_r}) \quad (1)$$

where σ_{i_r,j_f} is the STD of the distance between the raw position of marker i and the filtered position of marker j . We computed a σ_{dist} both for the pelvic markers and for the chest markers and chose a cutoff frequency that minimized the mean of these two values. A rigid body least-squares error fitting applied to the pelvic and chest markers served as a second filtering step for these markers [19].

Solving the inverse kinematics (IK) refers to finding the model joint variables [θ_1 , θ_2 , d_3 , θ_4 , θ_5 , d_6] given an observed mid-ankle, pelvis, and chest position. The transformation matrix describing the pelvis frame 3 in frame 0 is

$$T_0^3 = \begin{bmatrix} c_1c_2 & -s_1 & c_1s_2 & -d_3c_1s_2 \\ s_1c_2 & c_1 & s_1s_2 & -d_3s_1s_2 \\ -s_2 & 0 & c_2 & d_3c_2 \end{bmatrix} \quad (2)$$

where "s" and "c" denote the sine and cosine functions and the numeric subscript denotes a rotation angle θ_i . The first column of the transformation matrix in 2 is the unit vector pointing from the mid-ankle to the pelvis described in frame 0. This vector can be used to solve for θ_1 and θ_2 . The joint variable d_3 is the distance from the ankle to the pelvis. Likewise, the rotation matrix describing the chest frame 6 orientation in the pelvis frame 3 is

$$T_3^6 = \begin{bmatrix} c_4c_5 & -s_4 & c_4s_5 & -d_6c_4s_5 \\ s_4c_5 & c_4 & s_4s_5 & -d_6s_4s_5 \\ -s_5 & 0 & c_5 & d_3c_5 \end{bmatrix} \quad (3)$$

and θ_4 , θ_5 , and d_6 can be found from (3) in the same manner. The θ_2 , θ_4 , and θ_5 depicted in Fig. 2 and discussed throughout this paper are equal to those in (2) and (3). When computing the forward kinematics, or computing pelvis and chest position from the model joint variables, we add $\frac{3\pi}{2}$ to θ_2 , θ_4 , and θ_5 to make them consistent with the DH convention.

When computing orientation variables for the pelvis and chest, we used pelvic and chest frame definitions as in Fig. 3. Using the unit vectors for the pelvic frame, the pelvic orientations with respect to the fixed ankle frame 0 were computed from the body 1-2-3 rotation matrix,

$$R_0^{plv} = \begin{bmatrix} {}^0\hat{x}_{plv} {}^0\hat{y}_{plv} {}^0\hat{z}_{plv} \\ c_2c_3 & -c_2s_3 & s_2 \\ s_1s_2c_3 + s_3c_1 & -s_1s_2s_3 + c_3c_1 & -s_1c_2 \\ -c_1s_2c_3 + s_3s_1 & c_1s_2s_3 + c_3s_1 & c_1c_2 \end{bmatrix} \quad (4)$$

The columns of the rotation matrix are the pelvic frame unit vectors expressed in frame 0, denoted $[{}^0\hat{x}_{plv} {}^0\hat{y}_{plv} {}^0\hat{z}_{plv}]$. This type of rotation, known as a rotation-obliquity-tilt or ROT-sequence, has been shown to provide angles most consistent with clinical definitions used for pelvic orientation, especially when pelvic rotation and tilt angles are large [20]. The pelvic rotation ($\theta_{plv,r}$), obliquity ($\theta_{plv,o}$), and tilt ($\theta_{plv,t}$) are equal to θ_1 , θ_2 , and θ_3 in (4), respectively. Importantly, pelvic tilt as defined here is highly influenced by hip flexion.

The orientation of the chest frame is reported relative to the pelvic frame and uses a non-sequenced convention recommended by the International Society of Biomechanics (ISB) for describing relative spinal segment orientations. Under the convention, relative orientation between vertebrae,

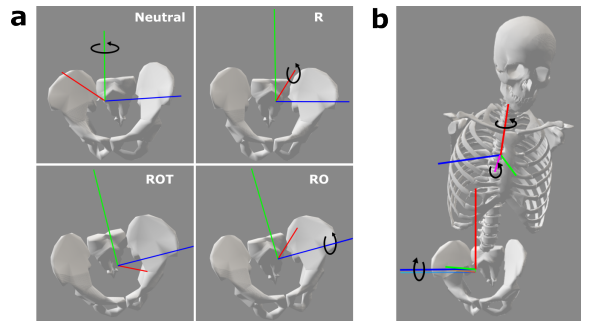


Fig. 3. Orientation descriptions for the pelvis and chest. **a:** The pelvic orientation is reported relative to the fixed base frame 0. The pelvic frame has been aligned with frame 0 in the top left "neutral" image. The first rotation is about the frame 0 x-axis (green axis, top left image) and is the pelvic rotation; the second rotation is about the resulting frame's y-axis (red axis, top right image) and is the pelvic obliquity; the third rotation is about the resulting frame's z-axis (blue axis, bottom right image) and is the pelvic tilt. The sequence is referred to as an ROT sequence. **b:** The chest orientation is relative to the pelvic frame, with lumbothoracic flexion/extension about a rightward pelvic z-axis (blue axis), lumbothoracic axial rotation about the chest's y-axis (red axis), and lumbothoracic lateral bending about a "floating" axis (pink axis).

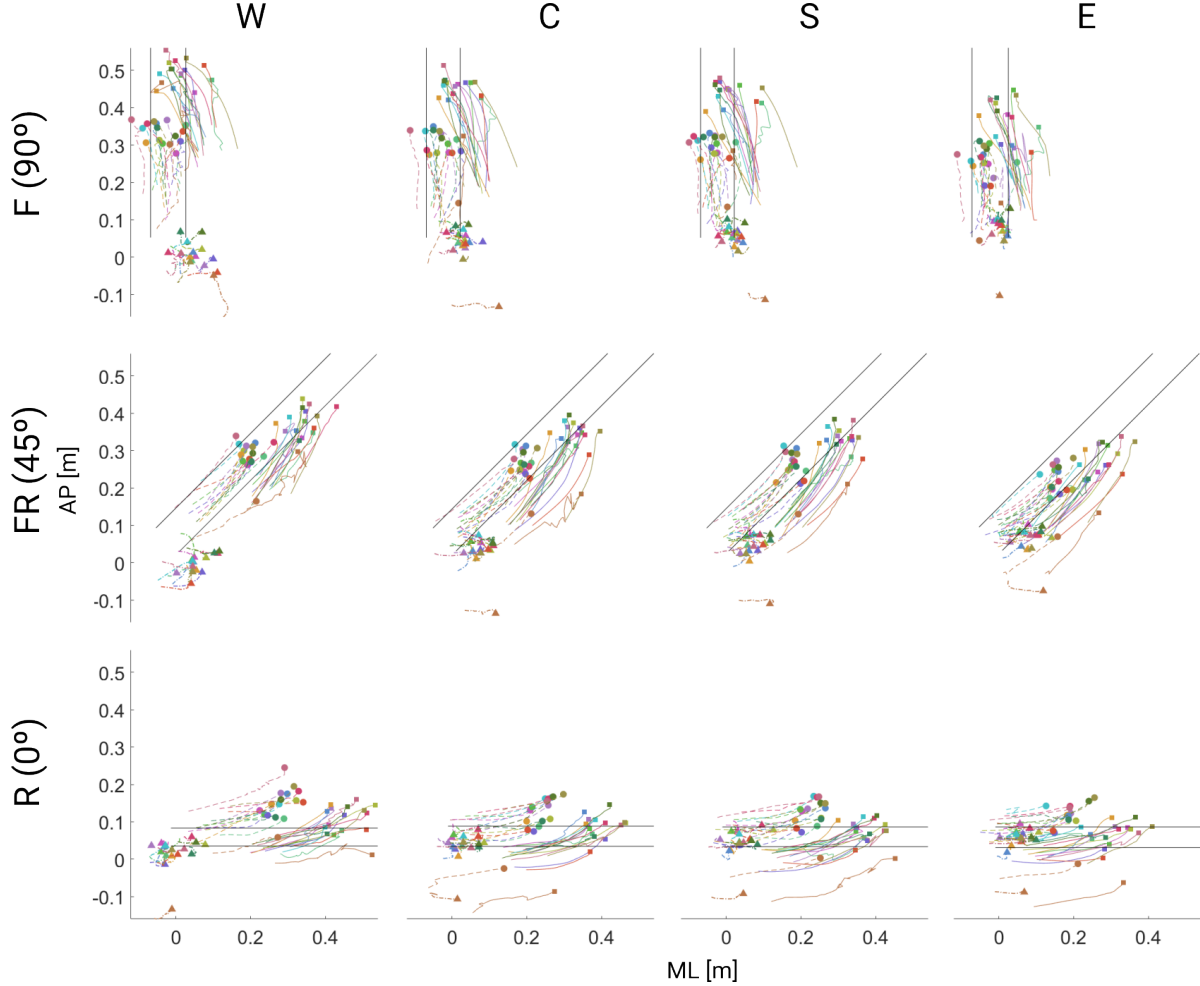


Fig. 4. Ground-plane trajectories of the pelvis (dashed-dotted lines terminated in triangles), chest (dashed lines terminated in circles), and shoulder of the right, reaching arm (solid lines terminated in squares) from 60%-100% reach progress are shown in the lab-fixed frame 0, which has an origin at the mid-ankle position. The x- and y-axes are the mediolateral (ML, rightwards positive) and anteroposterior (AP, forwards positive) directions, respectively. Reach target travel lines passed through the center of the subject-specific base of support, which was forward of the mid-ankle. The target travel lines for all subjects were located within the boundaries shown as black lines. Projecting onto the target travel line, the reaching shoulder moved further outwards than the chest for all subjects at all reach target directions and heights (waist- (W), chest- (C), shoulder- (S), and eye-level (E)). Chest and shoulder trajectories for the cohort were similar, with the average lock-step Euclidean distance between a subject's trajectory and other subject trajectories being much less than the average trajectory length. Backward movement of the pelvis increased with decreasing target height for the forward (F) and front-right (FR) directions. For the rightward (R) direction, the pelvis lateral movement increased with increasing target height. Chest and right shoulder excursion increased with decreasing target height in all directions. Notable forward movement of the chest is seen for righwards reaches, especially for waist-level targets.

spinal segments, or across the spine is described with flexion/extension, axial rotation, and lateral bending angles [21], [22]. We compute lumbothoracic flexion/extension about the pelvic z-axis (\hat{z}_{plv}), lumbothoracic axial rotation about the chest's y-axis (\hat{y}_{ch}), and lumbothoracic lateral bending about a "floating" axis (\hat{f}) obtained as the cross product of the chest's y-axis and pelvic z-axis (Fig. 3). These angles are most easily computed numerically, using

$$\hat{f} \cdot \hat{y}_{plv} = \cos(\theta_{ch,f}) \quad (5)$$

$$\hat{f} \cdot \hat{z}_{ch} = \cos(\theta_{ch,r}) \quad (6)$$

$$\hat{z}_{plv} \cdot \hat{y}_{ch} = \cos(\theta_{ch,b}) \quad (7)$$

We denote the flexion/extension, axial rotation, and lateral bending angles as $[\theta_{ch,f}, \theta_{ch,r}, \theta_{ch,b}]$.

D. Parameterizing Movement Progression

Intra- or inter-subject trajectories can be compared at a given value of a chosen progression parameter. Using normalized time as the parameter, one can compare postural variables at equivalent normalized time points, e.g. at 10% of the total temporal reach progression. Alternatively, as the task places constraints on the hand trajectory, normalized hand displacement could be used as the progression parameter. Specifically, we define the reach progression (RP) as the distance from the center of the BoS to the ground-plane projection of the hand normalized by the maximum such distance achieved in the reach. To determine whether using time or RP as the progression parameter better captures similar movement patterns between subjects, we used Lock-Step Euclidean Distance (LSED) to compute normalized similarities for the pelvis, chest, and reaching shoulder trajectories with both progression

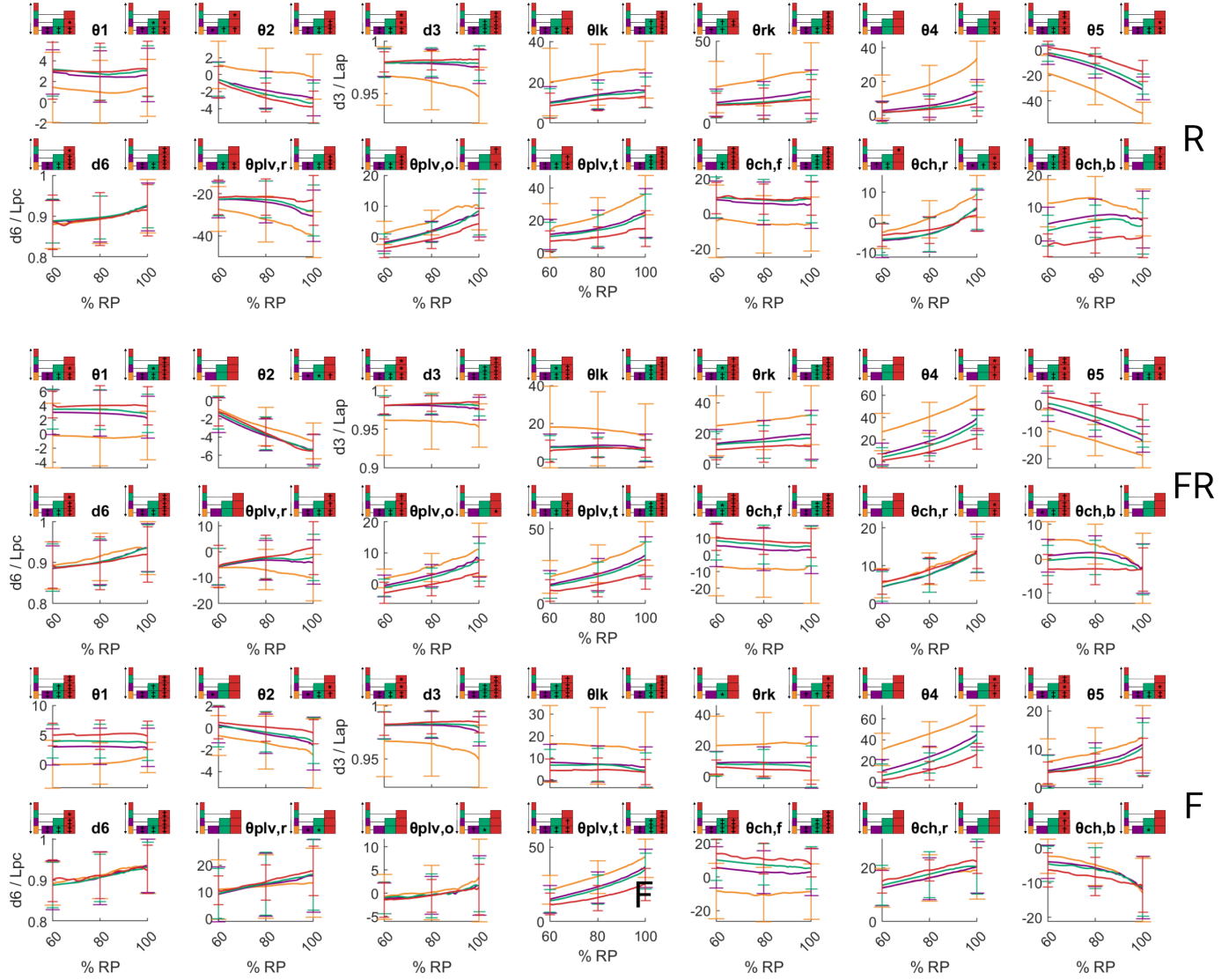


Fig. 5. For the forward (F), front-rightward (FR), and rightward (R) reaching directions, joint variable mean trajectories are plotted against percent reaching progression (RP) of the reach, with waist- (orange), chest- (purple), shoulder- (green), and eye-level (red) trajectories shown in different colors. Error bars show ± 1 standard deviation. X-axis ticks mark 60%, 80%, and 100% RP. Y-axes are in degrees unless otherwise noted. Colored grids present significant differences between reach heights; in each row, the variable value for the reach height corresponding to the color of the leftmost cell is compared to other reach heights in the row, with cell color indicating reach height. Significant differences with reach height are indicated in the cell of the compared reach height using symbols (* for $p < 0.05$, † for $p < 0.01$, and ‡ for $p < 0.001$).

parameters. LSED measures the average distance between corresponding points on two trajectories. If we denote two trajectories as trajectory A and B, let each trajectory have m corresponding points with point i on both trajectories denoted a_i and b_i , and the Euclidean distance between these points denoted $dist_2(a_i, b_i)$, then the LSED is

$$Eu(A, B) = \frac{1}{m} \sum_{i=1}^m dist_2(a_i, b_i) \quad (8)$$

For each subject, we computed a mean pelvis, chest, and shoulder trajectory for each direction/height combination by averaging corresponding points from the 3 trials. Trajectories corresponding to 60%-100% RP were analyzed, with either 401 points in steps of 0.01% RP or with 401 points equidistant in normalized time. We then computed a similarity between the mean pelvis, chest, and shoulder trajectories of subject i and

the cohort mean trajectories. Denoting the mean pelvis, chest, or shoulder trajectory for subject i as A_i and the cohort mean trajectory as M , then the normalized similarity value for the trajectory of subject i was computed as the LSED between the subject and cohort mean trajectories normalized by the cohort mean path length for the segment, l ,

$$S(A_i) = \frac{Eu(A_i, M)}{l} \quad (9)$$

E. Analyses Relating Model Joint Variables and Orientations to Shoulder Movement

In the first analysis, for each reach we quantified how model joint variables contributed to the end-pose position of the reaching arm's shoulder. We used the velocity Jacobian, ${}^0J_{v,RS}$, relating the model joint variable velocities with the velocity of the right shoulder in the base frame 0,

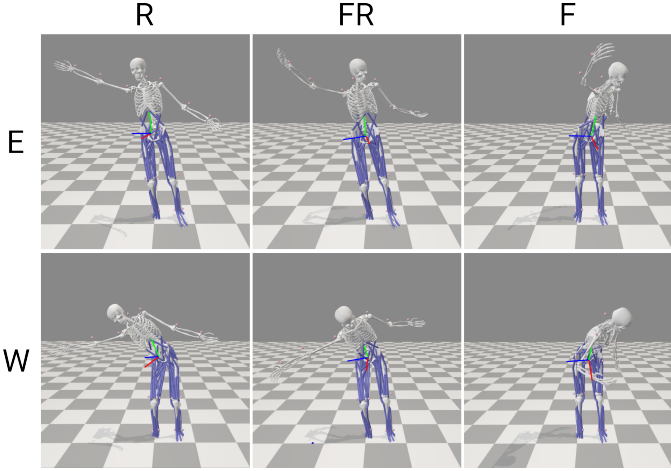


Fig. 6. Subject 12 poses at 100% reach progression (RP) for eye-level (top row; E) and waist-level (bottom row; W) targets for rightward (first column; R), front-rightward (second column; FR), and forward reaching (third column; F). When target height decreased, the magnitude of ankle-pelvis angles decreased and the magnitude of pelvis-chest angles, knee flexion, pelvic tilt and lumbothoracic lateral bending increased. Rightwards pelvic rotation increased for more rightwards targets and with decreasing target height in the 0° and 45° reach directions.

$${}^0 \begin{bmatrix} v_{RS,x} \\ v_{RS,y} \\ v_{RS,z} \end{bmatrix} = {}^0 J_{v,RS} \vec{q} = \begin{bmatrix} \sum_{j=1}^6 J_{1,j} \dot{q}_j \\ \sum_{j=1}^6 J_{2,j} \dot{q}_j \\ \sum_{j=1}^6 J_{3,j} \dot{q}_j \end{bmatrix} \quad (10)$$

where $\vec{q} = [\dot{\theta}_1, \dot{\theta}_2, \dot{d}_3, \dot{\theta}_4, \dot{\theta}_5, \dot{d}_6]^T$, \dot{q}_j denotes the j th element of \vec{q} , and $J_{i,j}$ is the element in the i th row and j th column of ${}^0 J_{v,RS}$. Integration of the individual terms in the summation in (10) over the time period spanning the outgoing portion of the reach yields the contribution of each joint to the shoulder's outgoing movement. For example, $\int_{t_i}^{t_f} J_{1,1} \dot{\theta}_1 dt$ yields the contribution of θ_1 to the x-component of the shoulder displacement. The analysis assumes the right shoulder is fixed in the chest frame 6 (Fig. 2).

In the second analysis, we approximate the contribution of the orientation variables to the reaching shoulder position by setting the end-pose, i.e., 100% RP, value of one orientation variable to its neutral pose value. We then quantified the resulting change in the shoulder position as a percent of the total shoulder displacement from its neutral position. First, we chose axes of rotation for each orientation variable. For pelvic orientation variables, we chose the pelvic frame axes about which the variables are defined, as in (4), see Fig. (3). As a result, setting orientation values to their neutral value assesses the effect of the pelvic orientation on the reaching shoulder position, assuming the body between the pelvis and reaching shoulder remains rigid. For lumbothoracic flexion/extension and lateral bending, we selected an axis of rotation parallel to the axis about which the variable was defined, but which passed through a variable-specific frame origin located halfway between the pelvic center or frame 3 origin and the chest center or frame 6 origin (Fig. 2). The lateral bending frame had an x-axis parallel to the floating axis about which it was defined. The flexion/extension frame had the same orientation as the pelvic frame. The axis of rotation

for lumbothoracic axial rotation was the chest frame y-axis.

To set an orientation variable to neutral, we expressed the end-pose shoulder position in the relevant frame. For pelvic rotation and obliquity, we then removed rotations later in the sequence, applied a negative rotation about the relevant axis to set the variable to neutral, and reapplied any removed rotations. The process for setting pelvic tilt and pelvis-relative chest orientations to zero required only applying a negative rotation about the relevant axis, as these angles were not defined as a sequence. Specifically, we transformed the end-pose right shoulder position as

$${}^0 \vec{p}_{(RS, rp=n)} = T_0^{plv} R_{z,-o} R_{x, rp} R_{y,o} R_{z,t} T_{plv}^0 {}^0 \vec{p}_{(RS)} \quad (11)$$

$${}^0 \vec{p}_{(RS, o=n)} = T_0^{plv} R_{z,-t} R_{y,o} R_{z,t} T_{plv}^0 {}^0 \vec{p}_{(RS)} \quad (12)$$

$${}^0 \vec{p}_{(RS, t=n)} = T_0^{plv} R_{z,t} T_{plv}^0 {}^0 \vec{p}_{(RS)} \quad (13)$$

$${}^0 \vec{p}_{(RS, f=n)} = T_0^f R_{z,f} T_f^0 {}^0 \vec{p}_{(RS)} \quad (14)$$

$${}^0 \vec{p}_{(RS, b=n)} = T_0^b R_{x,b} T_b^0 {}^0 \vec{p}_{(RS)} \quad (15)$$

$${}^0 \vec{p}_{(RS, rc=n)} = T_0^{ch} R_{y,r} T_{ch}^0 {}^0 \vec{p}_{(RS)} \quad (16)$$

$$(17)$$

where ${}^0 \vec{p}_{(RS)}$ is the end-pose right shoulder position in frame 0, $R_{x,i}$, $R_{y,i}$, and $R_{z,i}$ designate the basic rotation matrices specifying rotations around the x-, y-, and z-axes by the subscripted angle i , subscripts [rp, o, t, f, b, rc] denote $[\theta_{plv,r}, \theta_{plv,o}, \theta_{plv,t}, \theta_{ch,f}, \theta_{ch,b}, \theta_{ch,r}]$, respectively, $(T_0^{plv}, T_0^f, T_0^b, T_0^{ch})$ and $(T_{plv}^0, T_f^0, T_b^0, T_c^0)$ denote the transformation matrices from the pelvic, flexion/extension, lateral bending, and chest frames to frame 0 and their inverses, respectively, and ${}^0 \vec{p}_{(RS, \theta=n)}$ is the new shoulder position with the designated orientation variable θ set to its neutral value.

In the third analysis, we quantified the indirect contributions of ankle-pelvis angles on the reaching shoulder movement for waist-level reaches, with the hypothesis that subjects used the lower limbs to "counterbalance" the torso mass for waist-level reaches. The static inverted pendulum model of stance predicts that if the ground-plane projection of the body's COM, i.e, the center of gravity (COG), leaves the BoS, instability requiring a compensatory step or leading to a fall will result [23]. If the COM of the lower limbs and pelvis moves away from the reach target, the COM of the torso can move further towards the reach target before the COG reaches the edge of the BoS. For each waist-level reach in a given direction, we swapped each subject's observed ankle-pelvis angles with the subject's mean ankle-pelvis angles observed for all eye-level reaches in the same reach direction. We then computed new pelvis-chest angles (θ_4, θ_5) that would preserve the COG position and the resulting change in the reaching shoulder displacement.

F. Statistical Analysis

For the primary reach directions ($0^\circ = R$, $45^\circ = FR$, $90^\circ = F$), differences between the subject mean kinematic model joint variables at different reaching heights were assessed using a two-way repeated measures analysis of variance (rmANOVA) in R. The within-subjects factors were reaching height and

reaching direction. The dependent variable was the mean of a kinematic joint variable, pelvis or chest orientation angle, or a knee flexion angle at a certain percent progression through the movement. Extreme outliers were removed from the analysis. If needed, variables were transformed to achieve normality of residuals. We used post-hoc paired t-tests with Bonferroni correction to determine significant differences between levels. We evaluated differences at the 60% and 100% movement progression percentages. An identical analysis was performed for the shoulder displacement associated with a given joint variable or orientation variable.

III. RESULTS

In the starting period, the median model joint variables and orientation variables were normally distributed with cohort mean \pm STD values of $[\theta_1 : 3.57^\circ \pm 2.43^\circ; \theta_2 : 0.34^\circ \pm 0.76^\circ; d_3 : 1.00 \pm 0.00; \theta_4 : -2.70^\circ \pm 4.69^\circ; \theta_5 : 1.18^\circ \pm 1.59^\circ; d_6 : 1.00 \pm 0.00; \theta_{p,r} : -0.25^\circ \pm 5.32^\circ; \theta_{p,o} : -1.89^\circ \pm 3.03^\circ; \theta_{p,t} : 6.92^\circ \pm 7.05^\circ; \theta_{ch,f} : 9.79^\circ \pm 8.23^\circ; \theta_{ch,r} : 1.79^\circ \pm 4.69^\circ; \theta_{ch,b} : 2.46^\circ \pm 4.57^\circ]$. Reach distances normalized by subject height reported in ascending height (waist-, chest-, shoulder-, and eye-level) for 0° were [median \pm IQR: 0.498 ± 0.062 m, 0.487 ± 0.036 m, 0.475 ± 0.049 m, 0.435 ± 0.053 m], for 45° were [median \pm IQR: 0.517 ± 0.034 m, 0.507 ± 0.038 m, 0.495 ± 0.037 m, 0.450 ± 0.056 m], and for 90° were [median \pm IQR: 0.523 ± 0.030 m, 0.505 ± 0.023 m, 0.499 ± 0.025 m, 0.441 ± 0.040 m].

Parameterizing the pelvis, chest, and shoulder trajectories with RP yielded higher similarities, i.e., lower normalized LSED, than did a parameterization with time for all reach directions and heights. The mean values for normalized LSED parametrized by RP for all reach directions and heights were much larger for the pelvis (pelvis - min: 0.78; Q1: 0.88; med.: 1.08; Q3: 1.49; max.: 1.85) than for the chest (chest - min: 0.33; Q1: 0.34; med.: 0.38; Q3: 0.40; max.: 0.51) and shoulder (shoulder - min: 0.25; Q1: 0.27; med.: 0.28; Q3: 0.33; max.: 0.38). These values were significantly lower than from a parametrization by time, with average reductions in normalized LSED of (mean \pm STD - pelvis: $5.4\% \pm 3.3\%$; chest: $7.5\% \pm 2.6\%$; shoulder: $10.9\% \pm 3.1\%$), with statistically significant reductions for most reach direction/height combinations as assessed with pairwise t-tests (pelvis: 9/12; chest: 11/12; shoulder: 12/12).

As a result, in Fig. 5 we plot the model joint and orientation variables for all heights and the primary reaching directions against 60% to 100% RP. Symbols report significant differences between reach heights for p-values less than 0.05. Fig. 6 presents visualizations of one subject's end-pose posture for an eye- and waist-level reach in the 0° , 45° , and 90° reach directions using a full-body model with a rigid torso [24]. The visualization displays many key features of the effects of height and reach direction at 100% RP.

The contribution of the model joint variable and orientation variables to the displacement of the reaching shoulder are presented in Fig. 7. Statistically significant differences with height are shown in the figures. The results of the analysis of lower limb counterbalancing are presented in Fig. 8.

IV. DISCUSSION

Ankle-pelvis angles were generally smaller with decreasing target height or even directed away from the target for some waist-level reaches. Specifically, θ_1 decreased significantly with lower targets for forward (F) and front-rightward (FR) reaching and θ_2 magnitude decreased significantly with lower targets for rightward (R) reaching. Significant differences in θ_1 with height emerged early in the reach, i.e., by 60% RP, in all reach directions. For all targets, the shoulder moved forward, but surprisingly, the ankle-pelvis angles contributed little or negatively to forward right shoulder displacement. θ_1 contributions to forward shoulder movement tended to be more negative with lower reach target heights, a trend which was significant for forward reaching. Instead, pelvis-chest angles (θ_4 , θ_5) generated the large majority of the shoulder forward displacement for all reach target directions and heights (Fig. 7). In rightwards and front-rightwards reaching, θ_2 generated a substantial fraction of rightwards movement of the reaching shoulder which tended to increase with target height (Fig. 7).

In their double-inverted pendulum model of stance in the sagittal plane, Nashner et. al noted that subjects can reduce the effort needed to maintain balance by moving the pelvis in the opposite direction of the torso. In this case, the lower limb and pelvic masses partially counterbalance the gravity torque generated by the torso mass at the ankle [14]. This strategy can maintain balance while allowing for larger pelvis-chest angles. Indeed, older subjects performing the FRT leveraged counterbalancing by moving the pelvis further posteriorly and using greater hip flexion than younger subjects, with concurrent reductions in the AP displacement of the COP [5]. Our analysis revealed that ankle-pelvis angles had an important indirect effect on shoulder movement in all reach directions. Namely, smaller-magnitude ankle-pelvis angles for waist-level reaches enabled a large portion of the outwards and downwards movement of the reaching shoulder by enabling larger-magnitude pelvis-chest angles (Fig. 8).

The mid-ankle-to-pelvis distance (d_3) decreased with target height in all reach directions, while the left and right knee flexion increased with decreasing target height. The contribution of a shortening d_3 to downwards right shoulder movement tended to increase with decreasing target height, although it accounted for only a small fraction of downwards movement even for waist-level reaches. This suggests that knee flexion played a small role in lowering the reaching shoulder to the target and was more important for lower reaches. However, knee flexion may also have contributed to smaller θ_1 values (smaller anterior pelvic excursion) for lower targets in 90° and 45° reaching, as knee flexion likely moved the pelvis posteriorly. Both knee flexion and its asymmetry were also likely tightly linked to pelvic rotation and obliquity, given that the ground, lower limbs and pelvis can be modeled as a closed chain in double-support stance [25].

Pelvis-chest angles (θ_4 , θ_5) increased with decreasing target height in the 0° , 45° , and 90° reach directions. θ_4 and θ_5 generally changed substantially throughout the reach, but significant differences with reach height often emerged early in the reach, or by 60% RP. Concerning reaching shoulder

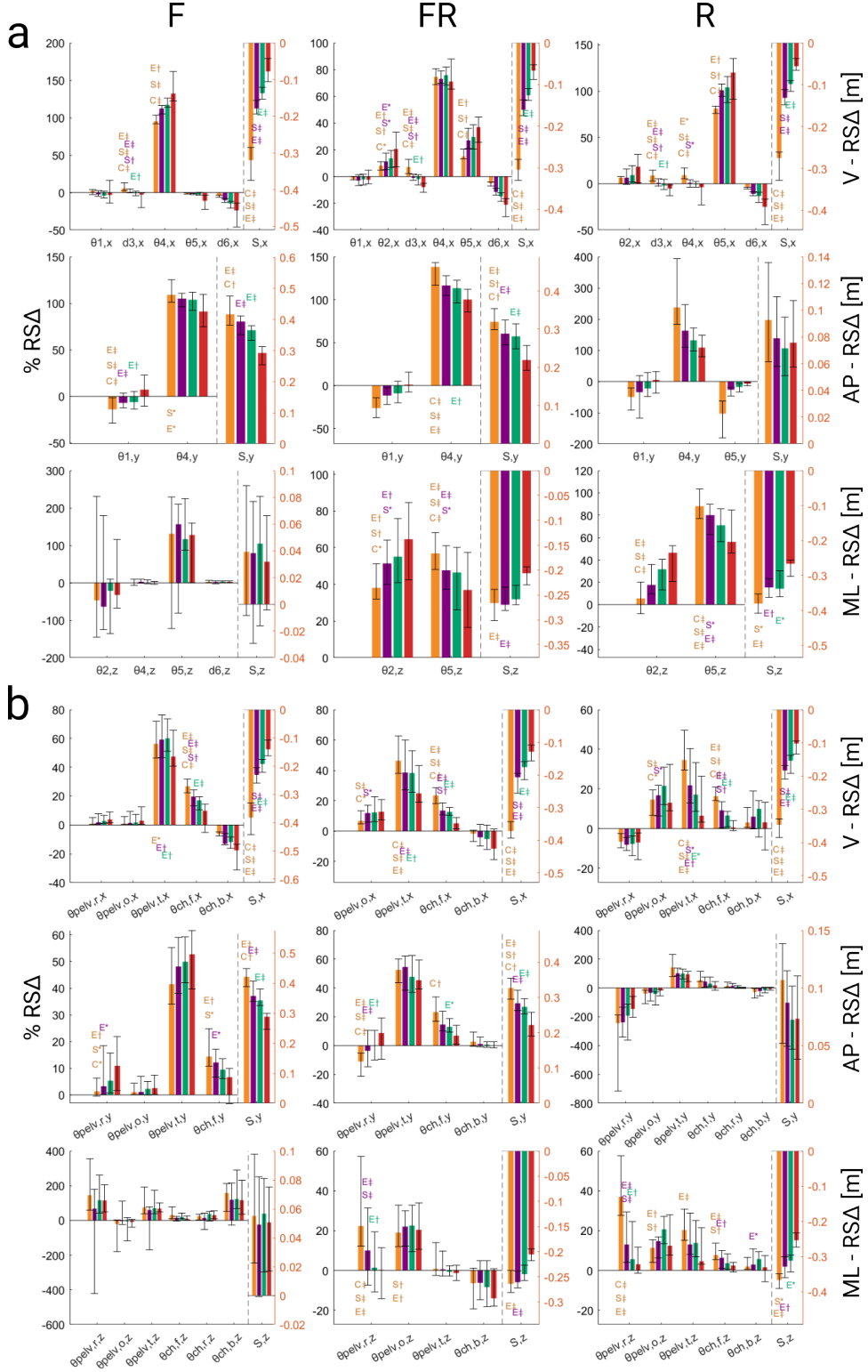


Fig. 7. Bars show the median contribution of selected **a.)** joint variables and **b.)** orientation variables to the reaching shoulder displacement as a percentage of the reaching shoulder displacement (% RSA Δ). The rightmost bar group in each plot shows the reaching shoulder displacement (S) in meters, which was measured from the pose nearest to the neutral pose after the appearance of the virtual reaching target to 100% reach progress. Data for the rightmost bar group, separated from other bar groups by a vertical dashed line, uses the right y-axis. Values for waist- (orange), chest- (purple), shoulder- (green), and eye-level (red) reaches are shown in different colors. From left to right, columns show forward (F), forward-right (FR), and right (R) reach directions. From top to bottom, rows correspond to x-axis (vertical, V), y-axis (anteroposterior, AP), and z-axis (mediolateral, ML) shoulder displacement components. Error bars extend to the 1st and 3rd quartile. Each plot shows only joint variables which contributed more than 5% to shoulder displacement, including the error bars. Statistically significant differences between reach heights are indicated above each bar. The letter color and position over a bar indicates the first reach height in the comparison, the letter indicates the compared reach height (C = chest, S = shoulder, E = eye), and significance is indicated using symbols (* for $p < 0.05$, † for $p < 0.01$, and ‡ for $p < 0.001$). As forward and lateral displacements were occasionally very small for R and F targets, respectively, % RSA Δ values could be very large; for this reason, statistical analyses were not performed for these components in these directions. Note that y-axes differ by plot when comparing values between plots.

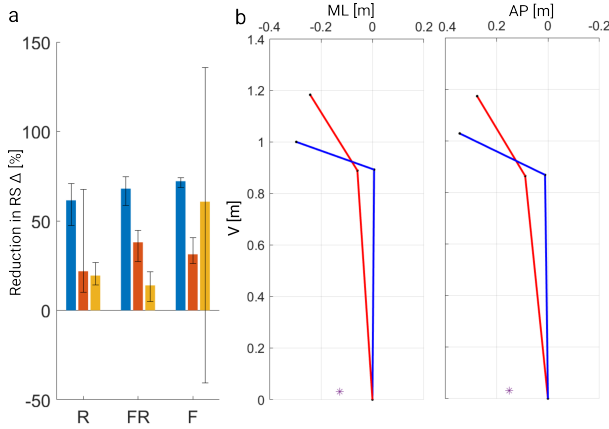


Fig. 8. **a:** We substituted larger, subject-specific eye-level ankle-pelvis angles in waist-level reaches and computed pelvis-chest angles that preserved the center of gravity (COG). Smaller resultant pelvis-chest angles lead to large reductions in reaching shoulder displacement, highlighting the importance of subtle ankle-pelvis angle changes with target height. Bars show the median percent reductions in reaching shoulder displacement ($RS\Delta$) components (vertical (x) = blue; antero-posterior (y) = red; mediolateral (z) = yellow) after the manipulation. Data is shown for the rightward (R), front-rightward (FR), and forward (F) reach directions. Error bars extend to the first and third quartile. **b:** Representative reaches showing the kinematic skeleton for the observed posture (blue) for a rightwards (left) and forwards (right) waist-level reach and the resulting posture when eye-level ankle-pelvis angles are substituted (red) and the center of gravity (COG; purple star) is preserved. The kinematic skeletons include two links, one from the mid-ankle to the pelvis and one from the pelvis to the chest.

movement, pelvis-chest angles generated the large majority of both forwards and downwards movement and a substantial portion of lateral movement for all reach target directions and heights, see Fig. 7. Pelvis-chest distance (d_6) generally slightly increased throughout the reach, generating some upwards movement of the reaching shoulder and contributing little to outwards movement of the shoulder (Fig. 7).

Rightwards pelvic rotation increased for more rightwards targets. Pelvic tilt, which is largely influenced by hip flexion, increased with decreasing target height in all reach directions. Pelvic tilt generated a majority of the downwards movement of the reaching shoulder for all forward targets. For forward-right and rightward targets, pelvic tilt generated a larger fraction of downward movement for lower targets. Pelvic tilt was also important for forward movement of the shoulder in all reach directions. Both pelvic rotation and tilt also generated substantial fractions of rightward shoulder movement for waist-level rightward reaches. In this case, the fraction of lateral movement generated by pelvic rotation captures both the direct effect of pelvic rotation on the shoulder position and its effect on the hip flexion (i.e., pelvic tilt) axis. For low rightward reaches, rightward pelvic rotation oriented the axis containing the two hip joint centers, about which hip flexion occurs, such that hip flexion contributed to forward, lateral, and downward movement of the shoulder (Figs. 5, 7). Shoulder forward displacement for low, rightward targets (Fig. 4) likely represents a compromise between increasing forward movement of the chest away from the target in order to move the shoulder downwards and laterally towards the

target. Subjects showed the greatest rightwards pelvic rotation in early rightwards reaching, likely to view targets early in the movement. Pelvic obliquity generated a modest fraction of downwards and lateral movement of the reaching shoulder for rightward and front-rightward targets.

In all reach directions, lumbothoracic flexion (negative $\theta_{ch,f}$) was typically observed throughout the reach for waist-level targets, whereas extension was observed for higher targets. Lumbothoracic extension also generally increased with increasing target height. However, some flexion occurred throughout the reach for almost all targets, such that $\theta_{ch,f}$ moved the shoulder forward and downward, an effect which increased in importance for lower targets (Fig. 7). A similar height-dependent trend was seen for the effect of spinal flexion on forward shoulder movement. Lumbothoracic axial rotation ($\theta_{ch,r}$) generally was leftwards and became more leftwards throughout the reach for all target reach directions and heights. However, it contributed little to right shoulder displacement. Prior work has noted reductions in the FRT reach distance in the elderly and speculated that reductions in lumbothoracic axial rotation may have played a role [11], [5]. The mean lumbothoracic axial rotation for forward, shoulder-level reaches observed here closely matches those previously seen in young, healthy subjects [11]. Therefore, our analysis suggests elements of the postural coordination other than lumbothoracic axial rotation, such as greater posterior pelvic displacement or more conservative COP displacement due to muscular weakness or an abundance of caution may explain reduced FRT scores in the elderly. Rightwards lumbothoracic axial rotation was typically seen only in early and middle (60-80% RP) rightwards (R) reaching, where similar to pelvic rotation it may have aided in early viewing of rightwards targets. Lumbothoracic lateral bending ($\theta_{ch,b}$) rightwards trended towards increasing with decreasing target height for rightwards targets. Lateral bending made small contributions to downward and lateral shoulder movement for lower rightwards (R) targets. Lumbothoracic lateral bending was typically of small magnitude (slightly leftwards) for front-rightwards (FR) reaching and leftwards for forward (F) reaching, where it typically acted against observed downward shoulder movement.

V. CONCLUSION AND LIMITATIONS

For forward, shoulder-level targets, the observed joint and orientation variable coordination patterns and a predominance of the "hip strategy" were consistent with the literature [11], [5], [26]. We extended these findings to quantify the relative importance of the ankle-pelvis, pelvis-chest, and orientation angles when reaching to targets in different directions and heights. To displace the shoulder forwards to all forward (F, FR) targets, pelvis-chest angles and pelvic tilt played a key role and ankle-pelvis angles did not, consistent with a "hip strategy." Ankle-pelvis angles played an important, height-dependent role in laterally displacing the shoulder to rightward (R) targets, perhaps because in shoulder-width stance the COM can move further along the wider ML dimension of the BoS. When considering balance and COG position, reaching lower targets in any direction required smaller ankle-pelvis angles to

enable greater pelvis-chest angles that could lower the shoulder. This highlights how subtle changes in pelvis positioning can determine feasible postures while reaching. Knee flexion played a small role in moving the shoulder downwards to lower targets. Pelvic tilt and lumbothoracic flexion were key in moving the reaching shoulder forward and downward to all targets. Pelvic rotation and tilt were coordinated to contribute to lateral shoulder displacements for low R targets, whereas pelvic obliquity contributed to lateral shoulder movement for all lateral targets. Lumbothoracic lateral bending made small contributions to move the shoulder rightwards for R targets or forwards for F targets, but otherwise acted against downward shoulder movement. Lumbothoracic axial rotation contributed little to the reaching shoulder's movement. These observations highlight how movement restrictions in impaired populations may, or may not, affect the reaching workspace.

Subjects reached using an ulnar wrist marker, which introduced small differences from the more functionally relevant palm or finger position. We used approximated axes of rotation to estimate the contribution of lumbothoracic flexion/extension and lateral bending to right shoulder movement, introducing a source of error. We quantified the contribution of model joint variables to the reaching shoulder's movement. With a more comprehensive kinematic model and marker set, one could integrate the Jacobian to compute the contribution of anatomically relevant joints, such as the orientation of individual spinal segments, to the reaching hand's movement instead of to the shoulder. This approach could quantify how joint movement limitations in impaired populations affect goal-oriented reaching movements. As noted, gaze requirements, stance, and load during a reach can affect postural coordination.

Despite the specific context for reaches in this experiment, the results presented here provide widely applicable insight into how postural coordination can support upper limb tasks performed throughout the reaching workspace. We believe that this information can help guide future clinical research and therapy using upper limb tasks for postural rehabilitation.

REFERENCES

- [1] A. Logan et al., "Standing Practice In Rehabilitation Early after Stroke (SPIRES): A functional standing frame programme (prolonged standing and repeated sit to stand) to improve function and quality of life and reduce neuromuscular impairment in people with severe sub-acute stroke-a protocol for a feasibility randomised controlled trial," *Pilot Feasibility Stud.*, vol. 4, no. 1, Apr. 2018, doi: 10.1186/s40814-018-0254-z.
- [2] J. Bernhardt, H. Dewey, A. Thrift, J. Collier, and G. Donnan, "A very early rehabilitation trial for stroke (AVERT): Phase II safety and feasibility," *Stroke*, vol. 39, no. 2, pp. 390–396, Feb. 2008, doi: 10.1161/STROKEAHA.107.492363.
- [3] R. Dewar, S. Love, and L. M. Johnston, "Exercise interventions improve postural control in children with cerebral palsy: A systematic review," *Dev. Med. Child Neurol.*, vol. 57, no. 6, pp. 504–520, Jun. 2015, doi: 10.1111/dmcn.12660.
- [4] C. M. Dean and R. B. Shepherd, "Task-related training improves performance of seated reaching tasks after stroke: A randomized controlled trial," *Stroke*, vol. 28, no. 4, pp. 722–728, 1997, doi: 10.1161/01.STR.28.4.722.
- [5] L. de Waroquier-Leroy et al., "The Functional Reach Test: Strategies, performance and the influence of age," *Ann. Phys. Rehabil. Med.*, vol. 57, no. 6, pp. 452–464, Aug. 2014, doi: 10.1016/j.rehab.2014.03.003.
- [6] L. Heyman et al., "Clinical characteristics of impaired trunk control in children with spastic cerebral palsy," *Res. Dev. Disabil.*, vol. 34, no. 1, pp. 327–334, Jan. 2013, doi: 10.1016/j.ridd.2012.08.015.
- [7] S.-Y. Yu and B. J. Martin, "Upper Body Coordination in Reach Movements," in *Digit. Human Model. Des. Eng. Conf.*, Jun. 2008, doi: 10.4271/2008-01-1917.
- [8] N. J. Delleman, A. J. S. Hin, and T. K. Tan, "Postural Behaviour in Static Reaching Sideways," *SAE Trans.*, vol. 112, pp. 733–736, Nov. 2003, [Online]. Available: <http://www.jstor.org/stable/44699734>.
- [9] D. B. Chaffin, J. J. Faraway, X. Zhang, and C. Woolley, "Stature, age, and gender effects on reach motion postures," *Hum. Factors*, vol. 42, no. 3, pp. 408–420, 2000, doi: 10.1518/001872000779698222.
- [10] M. P. Reed, M. B. Parkinson, and D. W. Wagner, "Torso Kinematics in Seated Reaches," *SAE Tech. Pap.*, Jun. 2004, doi: 10.4271/2004-01-2176.
- [11] J. T. Cavanaugh et al., "Kinematic characterization of standing reach: comparison of younger vs. older subjects."
- [12] E. S. Jung, D. Kee, and M. K. Chung, "Upper body reach posture prediction for ergonomic evaluation models," *Int. J. Ind. Ergon.*, vol. 16, no. 2, pp. 95–107, Aug. 1995, doi: 10.1016/0169-8141(94)00088-K.
- [13] K. Abdel-Malek, J. Arora, R. Bhatt, K. Farrell, C. Murphy, and K. Kregel, "Santos: An integrated human modeling and simulation platform," in *DHM and Posturography*, Elsevier, 2019, pp. 63–77.
- [14] L. M. Nashner and G. McCollum, "The organization of human postural movements: A formal basis and experimental synthesis," 1985.
- [15] Y. Suzuki, T. Nomura, M. Casadio, and P. Morasso, "Intermittent control with ankle, hip, and mixed strategies during quiet standing: A theoretical proposal based on a double inverted pendulum model," *J. Theor. Biol.*, vol. 310, pp. 55–79, Oct. 2012, doi: 10.1016/j.jtbi.2012.06.019.
- [16] K. H. Kim, R. B. Gillespie, and B. J. Martin, "Negotiated control between the manual and visual systems for visually guided hand reaching movements," *J. Neuroeng. Rehabil.*, vol. 11, no. 1, Jun. 2014, doi: 10.1186/1743-0003-11-102.
- [17] Y. Xiang, J. S. Arora, and K. Abdel-Malek, "3D human lifting motion prediction with different performance measures," *Int. J. Humanoid Robot.*, vol. 9, no. 2, Jun. 2012, doi: 10.1142/S0219843612500120.
- [18] S. Schreven, P. J. Beek, and J. B. J. Smeets, "Optimising filtering parameters for a 3D motion analysis system," *J. Electromyogr. Kinesiol.*, vol. 25, no. 5, pp. 808–814, Oct. 2015, doi: 10.1016/j.jelekin.2015.06.004.
- [19] A. Cappello, P. F. La Palombara, and A. Leardini, "Optimization and smoothing techniques in movement analysis," *Int. J. Biomed. Comput.*, vol. 41, no. 3, pp. 137–151, Jun. 1996, doi: 10.1016/0020-7101(96)01167-1.
- [20] R. Baker, "Pelvic angles: a mathematically rigorous definition which is consistent with a conventional clinical understanding of the terms," *Gait Posture*, vol. 13, no. 1, pp. 1–6, Feb. 2001, doi: 10.1016/S0966-6362(00)00083-7.
- [21] E. S. Grood and W. J. Suntay, "A Joint Coordinate System for the Clinical Description of Three-Dimensional Motions: Application to the Knee," *J. Biomech. Eng.*, vol. 105, no. 2, pp. 136–144, May 1983, doi: 10.1115/1.3138397.
- [22] G. Wu et al., "ISB recommendation on definitions of joint coordinate system of various joints for the reporting of human joint motion—part I: ankle, hip, and spine," *J. Biomech.*, vol. 35, no. 4, pp. 543–548, Apr. 2002, doi: 10.1016/S0021-9290(01)00222-6.
- [23] A. L. Hof, "The 'extrapolated center of mass' concept suggests a simple control of balance in walking," *Hum. Mov. Sci.*, vol. 27, no. 1, pp. 112–125, Feb. 2008, doi: 10.1016/j.humov.2007.08.003.
- [24] S. R. Hamner, A. Seth, and S. L. Delp, "Muscle contributions to propulsion and support during running," *J. Biomech.*, vol. 43, no. 14, pp. 2709–2716, Oct. 2010, doi: 10.1016/j.jbiomech.2010.06.025.
- [25] Z. Svoboda, M. Janura, P. Kutilek, and E. Janurova, "Relationships between movements of the lower limb joints and the pelvis in open and closed kinematic chains during a gait cycle," *J. Hum. Kinet.*, vol. 50, no. 2, pp. 37–43, Jun. 2016, doi: 10.1515/hukin-2015-0168.
- [26] R. W. Bohannon, B. J. Myers, F. T. Tudini, J. T. Clark, and J. P. Manor, "Kinematics of shoulder, trunk, pelvis, and hip while reaching forward to progressively distant targets," *J. Bodyw. Mov. Ther.*, vol. 24, no. 3, pp. 221–226, Jul. 2020, doi: 10.1016/j.jbmmt.2020.03.003.